

Depth Profiles and the Geometric Exploration of Random Objects Through Optimal Transport

Paromita Dubey^{*1}, Yaqing Chen^{*2}, and Hans-Georg Müller^{†3}

¹Department of Data Sciences and Operations, Marshall School of Business,
University of Southern California

²Department of Statistics, Rutgers University

³Department of Statistics, University of California, Davis

Abstract

We propose new tools for the geometric exploration of data objects taking values in a general separable metric space (Ω, d) . Given a probability measure on Ω , we introduce *depth profiles*, where the depth profile of an element $\omega \in \Omega$ refers to the distribution of the distances between ω and the other elements of Ω . Depth profiles can be harnessed to define *transport ranks*, which capture the centrality of each element in Ω with respect to the entire data cloud based on optimal transport maps between depth profiles. We study the properties of transport ranks and show that they provide an effective device for detecting and visualizing patterns in samples of random objects and also entail notions of transport medians, modes, level sets and quantiles for data in general separable metric spaces. Specifically, we study estimates of depth profiles and transport ranks based on samples of random objects and establish the convergence of the empirical estimates to the population targets using empirical process theory. We demonstrate the usefulness of depth profiles and associated transport ranks and visualizations for distributional data through a sample of age-at-death distributions for various countries, for compositional data through energy usage for U.S. states and for network data through New York taxi trips.

Keywords: Metric space valued data; transport rank; transport median; quantiles; outlyingness; visualization of random objects; Wasserstein metric

^{*}Contributed equally to the paper.

[†]Research supported in part by NSF grant DMS-2014626

1 Introduction

Substantial efforts have been made over the last decades to quantify the center-outward ordering of data. While this is straightforward for univariate measurements, it is challenging for multivariate data due to the lack of a total ordering in \mathbb{R}^p for $p > 1$, not to speak of random objects, which refer to data that take values in general metric spaces. Statistical depth is a key concept to determine the centrality of multivariate data with respect to an underlying probability distribution, and has a long history and rich literature including Tukey’s halfspace depth (Tukey 1975), convex hull peeling depth (Barnett 1976), simplicial volume depth (Oja 1983), simplicial depth (Liu 1990), zonoid depth (Koshevoy and Mosler 1997), projection depth (Zuo and Serfling 2000), and spatial depth (Serfling 2002), as well as families of depths (Paindaveine and Van Bever 2013; Yang and Modarres 2018), with a recent review in Mosler and Mozharovskyi (2021). Choosing among different notions of depth, Zuo and Serfling (2000) and Dyckerhoff (2004) discussed desirable attributes regarding invariance, monotonicity, continuity and convexity; see Mosler (2013) for a more recent discussion. Depths constitute a versatile tool for descriptive and inferential statistics that has been employed, for example, to quantify outlyingness and deepest points, and also for data visualization, regression, classification and testing (Liu et al. 1999; Rousseeuw et al. 1999; Rousseeuw and Hubert 1999; Jörnsten 2004; Li and Liu 2004; Ghosh and Chaudhuri 2005; Li et al. 2012; Liu et al. 2013; Lange et al. 2014, among many others).

Notions of depths have also become popular in the analysis of functional data that consist of random functions. The various definitions of depths for functional data include two major classes of depths (Mosler and Mozharovskyi 2021), integrated depths (Nagy et al. 2016) and infimal depths (Mosler and Polyakova 2012; Mosler 2013). Integrated depths include integrals of cross-sectional univariate depths (Fraiman and Muniz 2001), modified band depth (López-Pintado and Romo 2009), modified half-region depth (López-Pintado and Romo 2011) and multivariate functional integrated depths (Claeskens et al. 2014), while depths of infimal type include band

depth (López-Pintado and Romo 2009), variations of functional Tukey depth (Dutta et al. 2011; De Micheaux et al. 2021), and half-region depth (López-Pintado and Romo 2011). We refer to Gijbels and Nagy (2017) for a comprehensive review; see also Nieto-Reyes and Battey (2016).

In this paper we go beyond multivariate and functional data, which are usually viewed as random elements taking values in a vector space, and consider more complex data that we refer to as random objects. Random objects reside in a space equipped with a metric or dissimilarity measure, which generally lacks a linear structure, and include data on finite- and infinite-dimensional manifolds such as the Wasserstein space of distributions or data in general Hadamard spaces (Lin and Müller 2021). Such data are increasingly common in data science and statistics. Notions of depths have been generalized to data on finite-dimensional manifolds, including circular and spherical data (Liu and Singh 1992), covariance or correlation matrices (Zhang 2002; Chen et al. 2018; Painsaveine and Van Bever 2018), Hermitian positive definite matrices (Chau et al. 2019) and set-valued data (Cascos et al. 2021). Distance-based lens depth was first introduced in multivariate settings (Liu and Modarres 2011) and has recently been extended to data in Riemannian manifolds and semimetric/metric spaces (Kleindessner and von Luxburg 2017; Cholaquidis et al. 2020; Geenens et al. 2021). Other very recent developments include an extension of Tukey’s depth to the case of random objects (Dai and Lopez-Pintado 2021) and an approach to nonparametric inference in metric spaces based on ball distance correlation (Wang et al. 2021).

Our primary goal is to develop a toolbox for exploring the geometry of random objects, which is crucial for modern data science applications. It turns out that the proposed tools can be harnessed to obtain a notion of data depth that differs substantially from existing notions of depth and thus offers an entirely new perspective. Previous approaches that focused on depth for data that are either not finite-dimensional or do not reside in a linear space adopted classical notions of depth for multivariate data as starting point, extending the same notions to more general spaces. In contrast, from the get-go we develop tools that are directly aimed at random objects in metric spaces; to our knowledge, the key notion of transport depth that we develop here

has so far not been considered even for classical structured linear spaces. Our starting point are depth profiles for each element in the space Ω that lend themselves to visualize random objects and in combination with optimal transport to quantify centrality and outlyingness. Depth profiles emerge as basic tools for the exploratory analysis of samples of random objects. Our methods are grounded in principled modeling and supported by theory. We develop sample-based estimators of the proposed notions of depth profiles, transport ranks and transport medians and establish their convergence to the corresponding population targets. For the theory challenges arise due to the nonlinearity of the underlying metric space and the dependence between the estimated depth profiles. We overcome these challenges by employing tools from empirical processes.

The *depth profiles* that are key to our approach are indexed by the elements $\omega \in \Omega$. Given ω , the depth profile at ω is the distribution of the distances between ω and the other elements of Ω , where this distribution is determined by the probability measure on Ω that governs the distribution of the random objects across Ω and generates the observed data. The depth profile thus associates a one-dimensional distribution with each $\omega \in \Omega$. Depth profiles indicate the relative location of ω within Ω , and for samples the relative location of ω within the data point cloud of random objects. A second key idea is to harness optimal transports between the distributions that constitute the depth profiles at different elements ω . These optimal transports then lead to the definition of a *transport rank* that constitutes a notion of depth and provides an outwards ordering for random objects. Transport ranks can also be used to identify the most central random objects, the *transport median set*, along with level sets and quantiles.

In Section 2, we introduce the key ingredients of our methodology, i.e., depth profiles, transport ranks and transport median sets. In Section 3, we describe their properties and basic features, for example, invariance under measure preserving and distance preserving maps and also introduce the notions of transport depth modes, level sets and quantiles. We propose sample-based estimators and establish asymptotic guarantees in Section 4 and then proceed to illustrate the efficacy and visualization of depth profiles and transport ranks with simulated multivariate

and distribution-valued data in Section 5. The potential of the new notions for data science is demonstrated through data applications in Section 6, featuring human mortality distributions, U.S. electricity generation compositions, and Manhattan Yellow Taxi trip records. Proofs, auxiliary results and additional data illustrations are in the Supplement.

2 Depth Profiles, Transport Ranks and Transport Median Set

To introduce and motivate the key notions for our approach, we assume that data and random objects of interest are situated in a totally bounded separable metric space (Ω, d) . Consider a probability space $(S, \mathcal{S}, \mathbb{P})$, where \mathcal{S} is the Borel sigma algebra on a domain S and \mathbb{P} is a probability measure. A random object X is an Ω -valued random variable, i.e., a measurable map $X: S \rightarrow \Omega$ and P is a Borel probability measure that generates the law of X , i.e., $P(A) = \mathbb{P}(\{s \in S : X(s) \in A\}) =: \mathbb{P}(X \in A) = \mathbb{P}(X^{-1}(A)) =: \mathbb{P}X^{-1}(A)$, for any Borel measurable $A \subseteq \Omega$. For any $\omega \in \Omega$, let F_ω denote the cumulative distribution function (cdf) of the distribution of the distance between ω and a random element X that is distributed according to P . In our notation, we suppress the dependence of F_ω on P .

Formally, for any $t \in \mathbb{R}$, we define the *depth profile* at ω as

$$F_\omega(t) = \mathbb{P}(d(\omega, X) \leq t), \quad (1)$$

so that F_ω is a one-dimensional distribution that captures the probability mass enclosed by a metric ball in Ω that has center ω and radius t , for all $t \geq 0$. Thus the depth profile at ω is the distribution of the distances that need to be covered to reach other elements of Ω when starting out at ω , as dictated by the distribution P of the random objects X . An element ω that is centrally located, i.e., close to most other elements, will have a depth profile with more mass near 0, in contrast to a distantly located or outlying element whose depth profile will assign mass farther away from 0. If depth profiles have densities, for a centrally located ω the density will

have a mode near 0, while the density near 0 will be small for a distantly located ω .

The collection of depth profiles $\{F_\omega : \omega \in \Omega\}$ represents the one-dimensional marginals of the stochastic process $\{d(\omega, X)\}_{\omega \in \Omega}$. These simple marginals uniquely characterize the underlying measure P if (Ω, d) is a metric space of strong negative type (Lyons 2013); see Proposition 1 below and Section S1 in the supplement for details. Our goal is to use these simple marginals to obtain information about the complex distribution of the random objects X . Empirical versions of these marginals serve as estimates of the depth profiles and are introduced below. A result concerning the basic set-up for depth profiles is as follows; the proof is in Section S1 in the supplement.

Proposition 1. *The stochastic process $\{d(\omega, X)\}_{\omega \in \Omega}$, for which the depth profiles $\{F_\omega : \omega \in \Omega\}$ as defined in (1) are the one-dimensional marginals, is well-defined. Suppose that for some $k > 0$, (Ω, d^k) is of strong negative type (Lyons 2013), i.e., $\int_\Omega \int_\Omega d^k(\omega, x) dP_1(\omega) dP_1(x) + \int_\Omega \int_\Omega d^k(\omega, x) dP_2(\omega) dP_2(x) - 2 \int_\Omega \int_\Omega d^k(\omega, x) dP_1(\omega) dP_2(x) \leq 0$ for all probability measures P_1, P_2 on Ω , where equality holds if and only if $P_1 = P_2$. Then $P_1 = P_2$ if and only if $F_\omega^{P_1}(u) = F_\omega^{P_2}(u)$ for all $\omega \in \Omega$ and $u \in \mathbb{R}$, where $F_\omega^{P_1}$ and $F_\omega^{P_2}$ are the depth profiles of ω with respect to P_1 and P_2 .*

Consider the depth profile F_X of a random object $X \in \Omega$, $F_X(u) = \mathbb{P}_{X'}(d(X, X') \leq u)$ where $\mathbb{P}_{X'}$ is the law of X' , an i.i.d. copy of X . For each ω , the push-forward map of F_ω to F_X , given by $F_X^{-1}(F_\omega(\cdot))$, determines the optimal transport from the depth profile F_ω to the depth profile F_X . Here and throughout F^{-1} denotes the quantile function corresponding to a cdf F , $F^{-1}(u) = \inf\{x \in \mathbb{R} : F(x) \geq u\}$, for $u \in (0, 1)$. We utilize the optimal mass transport map

$$H_{X,\omega}(u) = F_X^{-1}(F_\omega(u)) - u, \quad u \geq 0, \quad (2)$$

see, e.g., Ambrosio et al. (2008), to assign a measure of centrality to an element $\omega \in \Omega$ with

respect to P . When F_ω is continuous, by a change of variable, the integral

$$\int H_{X,\omega}(u) dF_\omega(u) = \int_0^1 \{F_X^{-1}(u) - F_\omega^{-1}(u)\} du \quad (3)$$

provides a summary measure of the mass transfer that takes place when transporting F_ω to F_X .

The utility of this notion is that if ω is more centrally located than X with regard to the measure P , we expect the mass transfer to be predominantly from left to right and the magnitude of the integral in (3) to reflect the outlyingness differential between ω and a random object X , $X \sim P$. For example, for distributions P that are symmetric around a central point ω_0 and assign less mass when moving away from ω_0 , we expect that the integral (3) with $\omega = \omega_\oplus$ is relatively large and the magnitude of the integral (3) is decreasing as the distance from ω_\oplus increases. This motivates to take the expected value of the integral in (3) to quantify the degree of centrality or outlyingness of an element ω and is illustrated in Figure 1 for the case where X is a bivariate Gaussian random variable with mean zero and covariance $\text{diag}(2, 1)$. For the points $x \in \{(0, 0), (2, 0), (4, 0), (6, 0)\}$ and $\omega = (2, 2)$, their corresponding depth profiles are depicted as densities f_x and f_ω in the left panel, where the distances from x to the rest of the data are seen to increase as x moves away from the origin, which is exactly what one expects. For $x \in \{(0, 0), (2, 0), (4, 0), (6, 0)\}$, the maps $H_{x,\omega}$ as per (2) to a fixed element $\omega = (2, 2)$ are in the right panel. For $\omega = (2, 2)$, mass moves to the left when transporting F_ω to F_x for $x \in \{(0, 0), (2, 0)\}$, which are closer to the origin, and moves to the right for $x \in \{(4, 0), (6, 0)\}$, which are farther away from the origin. Another example based on the U.S. electricity generation compositions in Section 6.2 is shown in Figure 2. From Maryland (MD), Massachusetts (MA), Louisiana (LA) to Rhode Island (RI), one moves from the center of the sample toward the boundary of the space. For $\omega = \text{New Jersey (NJ)}$, mass in the depth profiles mostly moves to the left when transporting F_ω to F_x for $x = \{\text{MD}, \text{MA}\}$ and moves to the right for $x = \text{RI}$.

This motivates the notion of *transport ranks* to measure centrality of an element $\omega \in \Omega$ with

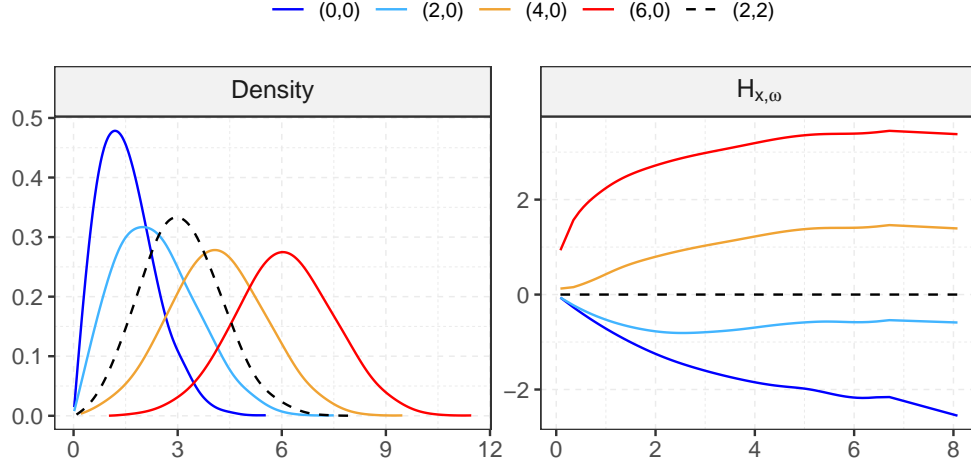


Figure 1: Left: Depth profiles, represented by the corresponding densities, at five points as indicated, with respect to a bivariate Gaussian distribution with mean zero and covariance $\text{diag}(2, 1)$. Right: Transport maps subtracted by identity $H_{x,\omega}$ as per (2) for $x \in \{(0, 0), (2, 0), (4, 0), (6, 0)\}$ and $\omega = (2, 2)$, where negative (positive) values indicate transport to the right (left).

respect to P as the $\text{expit}(\cdot)$ of the expected integrated mass transfer when transporting F_ω to F_X , where $P = \mathbb{P}X^{-1}$ where $\text{expit}(x) = e^x/(1 + e^x)$. Here the $\text{expit}(\cdot)$ transformation ensures that the proposed ranks are scaled to lie in $(0, 1)$ and it can be replaced by any other strictly monotone function from \mathbb{R} to $[0, 1]$. Formally,

$$R_\omega = \text{expit} \left[\mathbb{E} \left\{ \int_0^1 [F_X^{-1}(u) - F_\omega^{-1}(u)] du \right\} \right]. \quad (4)$$

The empirical transport rank of X_j with regard to the empirical measure of the entire sample $\{X_1, \dots, X_n\}$ is given by

$$\hat{R}_{X_j} = \text{expit} \left[\frac{1}{n} \sum_{i=1}^n \left\{ \int_0^1 [F_{X_i}^{-1}(u) - F_{X_j}^{-1}(u)] du \right\} \right]. \quad (5)$$

The empirical transport rank expresses the aggregated preference of X_j with respect to the data cloud. The greater the transport rank of X_j is, the more centered is X_j relative to the other

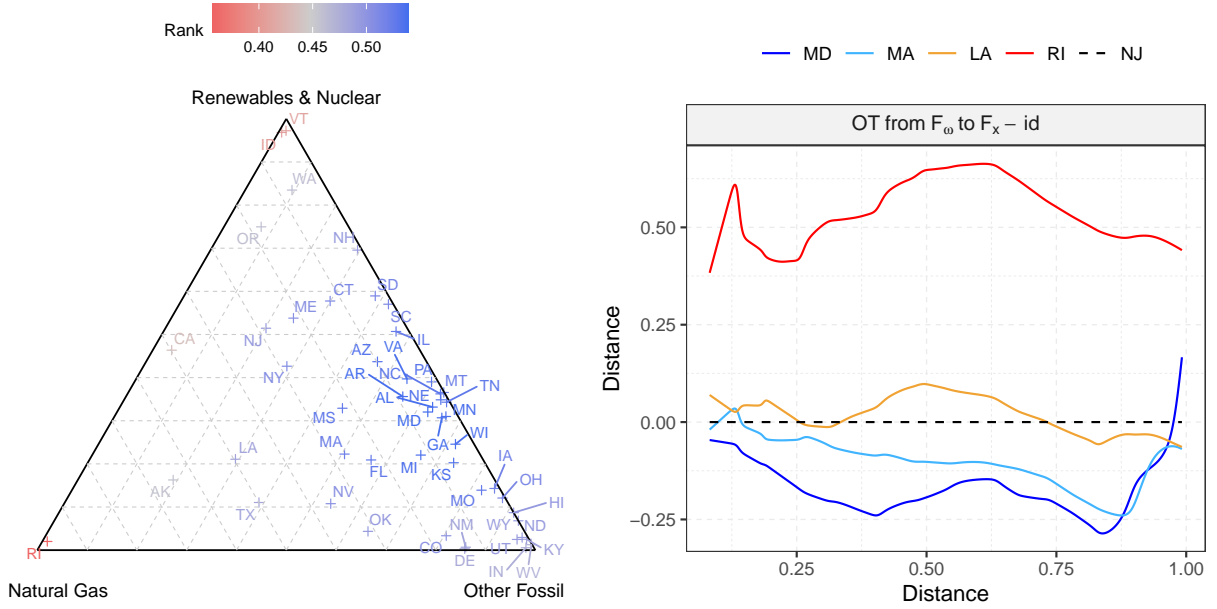


Figure 2: Left: Ternary plot of compositions of electricity generation in the year 2000 for the 50 states in the U.S., where the points are colored as per transport ranks. Right: Mass transport maps $H_{x,\omega}$ as per (2) for $x \in \{\text{MD}, \text{MA}, \text{LA}, \text{RI}\}$ and $\omega = \text{NJ}$.

sample elements. Equipped with an ordering of the elements of Ω by means of their transport rank we define the *transport median* set \mathcal{M}_\oplus of P as the collection of points in the support $\Omega_P \subset \Omega$ of P which have maximal transport rank and are therefore most central, i.e.,

$$\mathcal{M}_\oplus = \operatorname{argmax}_{\omega \in \Omega_P} R_\omega. \quad (6)$$

The depth profiles of the data objects together with the transport ranks and the transport median set are the key ingredients of the proposed toolkit to quantify centrality. These devices lend themselves to devise depth profile based methods for cluster analysis, classification and outlier detection, all of which are challenging when one deals with random objects.

3 Properties of Depth Profiles and Transport Ranks

We discuss here some desirable properties of depth profiles, transport ranks and the transport median set that are appropriately modified versions of analogous properties of classical ranks.

Lipschitz Continuity of Transport Ranks. By Lemma 1 in Section 4 the depth profiles $F_\omega(\cdot)$ and the associated quantile function representations $F_\omega^{-1}(\cdot)$ are uniformly Lipschitz in ω provided that the depth profiles have uniformly upper bounded densities with respect to the Lebesgue measure. This means that F_{ω_1} and F_{ω_2} are uniformly close to each other as long as ω_1 and ω_2 are close, and the distance between F_{ω_1} and F_{ω_2} is upper bounded by a constant factor of $d(\omega_1, \omega_2)$. Moreover transport ranks R_ω are uniformly Lipschitz in ω , see Lemma 2 below.

Invariance of Transport Ranks. Let $(\tilde{\Omega}, \tilde{d})$ be a metric space. A map $h: \Omega \rightarrow \tilde{\Omega}$ is isometric if $d(\omega_1, \omega_2) = \tilde{d}(h(\omega_1), h(\omega_2))$ for all $\omega_1, \omega_2 \in \Omega$. Theorem 1(a) establishes the invariance of depth profiles, and thereby of transport ranks, under isometric transformations. In Euclidean spaces this ensures that the depth profiles are invariant under orthogonal transformations.

Transport Modes and Center-Outward Decay of Transport Ranks. Consider a situation where the distribution P of X concentrates around a point $\omega_\oplus \in \Omega$. Specifically, if there exists an element $\omega_\oplus \in \Omega$ such that

$$F_{\omega_\oplus}(u) \geq F_\omega(u) \tag{7}$$

for any $\omega \in \Omega$ and any $u \in \mathbb{R}$ we refer to ω_\oplus as an Ω -valued *transport mode* of P . Condition (7) states that a d -ball of radius u around ω_\oplus contains more mass under P than a similar ball around any other point in Ω . According to Theorem 1(b), if P has a transport mode, then the transport rank of the transport mode must not be smaller than that of any other $\omega \in \Omega$ and therefore, the transport mode whenever it exists is contained in the transport median set. For distributions that concentrate around their unique Fréchet mean (Fréchet 1948), the Fréchet mean is the transport mode and hence is contained in the transport median set (Lunagómez et al. 2020). Theorem 1(c) provides a characterization of the radial ordering induced by the

transport rank for the special case where the data distribution on Ω has a transport mode ω_\oplus by considering curves of the form $\gamma: [0, 1] \rightarrow \Omega$ that originate from ω_\oplus , i.e. $\gamma(0) = \omega_\oplus$. According to Theorem 1(c), transport ranks are non-increasing along curves originating from a transport mode ω_\oplus , whenever P is such that the depth profiles decay systematically along the curve.

Characterization of the Measure P by Transport Ranks. Theorem 1(d) shows that when (Ω, d) is of strong negative type, the comprehensive set of all transport ranks $\{R_\omega\}_{\omega \in \Omega}$ uniquely characterizes the underlying measure.

Theorem 1. *For a separable metric space (Ω, d) the depth profiles F_ω and the transport ranks R_ω satisfy the following properties*

- (a) *Let $h: \Omega \rightarrow \tilde{\Omega}$ be a bijective isometric measurable map between (Ω, d) and $(\tilde{\Omega}, \tilde{d})$ and $P_h(\cdot) = P(h^{-1}(\cdot))$ the push-forward measure on $\tilde{\Omega}$. Then $F_{h(\omega)}^{P_h}(u) = F_\omega^P(u)$ for all $u \in \mathbb{R}$, hence $R_{h(\omega)}^{P_h} = R_\omega^P$, where $F_\omega^P(u) = \mathbb{P}(d(\omega, X) \leq u)$ and X is a Ω -valued random element such that $P = \mathbb{P}X^{-1}$, $F_{h(\omega)}^{P_h}(u) = \mathbb{P}(\tilde{d}(h(\omega), h(X)) \leq u)$, R_ω^P is the transport rank of ω with respect to P and $R_{h(\omega)}^{P_h}$ is the transport rank of $h(\omega)$ with respect to P_h .*
- (b) *If ω_\oplus is a transport mode of P as per (7), $R_{\omega_\oplus} \geq 1/2$. Moreover $R_{\omega_\oplus} \geq R_\omega$ for any $\omega \in \Omega$ and $\omega_\oplus \in \mathcal{M}_\oplus$.*
- (c) *Suppose ω_\oplus is a transport mode of P . Let $\gamma: [0, 1] \rightarrow \Omega$ be curve in (Ω, d) such that $\gamma(0) = \omega_\oplus$ and $F_{\gamma(s)}(u) \geq F_{\gamma(t)}(u)$ for all $u \in \mathbb{R}$ and $0 \leq s < t \leq 1$. Then $R_{\gamma(s)}(u) \geq R_{\gamma(t)}(u)$ whenever $0 \leq s < t \leq 1$.*
- (d) *Suppose (Ω, d) is of strong negative type (Lyons 2013), i.e., $\int_\Omega \int_\Omega d(\omega, x) dP_1(\omega) dP_1(x) + \int_\Omega \int_\Omega d(\omega, x) dP_2(\omega) dP_2(x) - 2 \int_\Omega \int_\Omega d(\omega, x) dP_1(\omega) dP_2(x) \leq 0$ for all probability measures P_1, P_2 on Ω , where equality holds if and only if $P_1 = P_2$. Then $P_1 = P_2$ if and only if $R_\omega^{P_1} = R_\omega^{P_2}$ for all $\omega \in \Omega$, where $R_\omega^{P_1}$ and $R_\omega^{P_2}$ are the transport ranks of ω with respect to P_1 and P_2 .*

The set of maximizers of R_ω in Ω_P constitutes the transport median set defined in (6). Observing that the function R_ω is uniformly continuous in ω by Lemma 2, the transport median set is guaranteed to be non-empty whenever Ω_P is compact. If Ω is a length space that is complete and locally compact, applying the Hopf–Rinow theorem, Ω is a geodesic space, and if Ω_P is any bounded closed subset of Ω , then it is guaranteed to be compact.

Equipped with an ordering of the elements of Ω in terms of their transport ranks, it is natural to consider level sets of the form $L_\alpha = \{\omega \in \Omega : R_\omega = \alpha\}$ and nested superlevel sets $L_\alpha^+ = \{\omega \in \Omega : R_\omega \geq \alpha\}$. By definition, $L_{\alpha_1}^+ \subseteq L_{\alpha_2}^+$ whenever $\alpha_1 \geq \alpha_2$. Due to the continuity of R_ω (see Lemma 2), the sets L_α and L_α^+ are closed. Moreover when (Ω, d) is a bounded, complete and locally compact length space, by the Hopf–Rinow theorem (Chavel 2006) L_α and L_α^+ are compact as well. There are numerous important applications of level sets and superlevel sets of random objects, for example superlevel sets L_α^+ can be viewed as depth regions and level sets can be used to define *depth quantile sets*. These can be viewed as a generalization of univariate quantiles to the case of random objects. Specifically, a ζ -level depth quantile set can be defined as L_α such that $P(X \in L_\alpha^+) = \zeta$, for $\zeta \in (0, 1)$. Complements of superlevel sets can be used to identify potential outliers by highlighting observations with low transport ranks. They can be also employed for data trimming by excluding points which have transport ranks lower than a threshold α ; one then might consider maximizers of R_ω over trimmed versions of Ω_P to obtain trimmed analogues of the transport median set \mathcal{M}_\oplus .

4 Estimation and Large Sample Properties

While so far we have introduced the notions of profile depth, transport rank and transport median sets at the population level, in practice one needs to estimate these quantities from a data sample of random objects $\{X_i\}_{i=1}^n$, i.e., a sample of n independent realizations of X . For

estimating the depth profiles F_ω , $\omega \in \Omega_P$, we consider the empirical estimates

$$\widehat{F}_\omega(t) = \frac{1}{n} \sum_{i=1}^n \mathbb{I}\{d(\omega, X_i) \leq t\}, \quad t \in \mathbb{R}. \quad (8)$$

Replacing expectations with empirical means and using estimated depth profiles \widehat{F}_{X_i} as surrogates of F_{X_i} , we obtain estimates for the transport rank of $\omega \in \Omega$ defined in (4) as

$$\widehat{R}_\omega = \text{expit} \left[\frac{1}{n} \sum_{i=1}^n \left\{ \int_0^1 [F_{X_i}^{-1}(u) - F_{X_j}^{-1}(u)] du \right\} \right]. \quad (9)$$

The term $\int_0^1 [\widehat{F}_{X_i}^{-1}(u) - \widehat{F}_\omega^{-1}(u)] du$ provides a comparison of the outlyingness of ω and of X_i ; mass movement predominantly to the right (left) indicates that ω is more central (outlying) compared to X_i , respectively. Finally we define the estimated transport median set $\widehat{\mathcal{M}}_\oplus$ as

$$\widehat{\mathcal{M}}_\oplus = \underset{\omega \in \{X_1, X_2, \dots, X_n\}}{\text{argmax}} \quad \widehat{R}_\omega. \quad (10)$$

To obtain asymptotic properties of these estimators and convergence towards their population targets, we require the following assumptions.

(A1) Let $N(\varepsilon, \Omega, d)$ be the covering number of the space Ω with balls of radius ε and $\log N(\varepsilon, \Omega, d)$ the corresponding metric entropy, which is assumed to satisfy

$$\varepsilon \log N(\varepsilon, \Omega, d) \rightarrow 0 \quad \text{as} \quad \varepsilon \rightarrow 0. \quad (11)$$

(A2) For every $\omega \in \Omega$ assume that F_ω is absolutely continuous with continuous density f_ω and let $\underline{\Delta}_\omega = \inf_{t \in \text{support}(f_\omega)} f_\omega(t)$ and $\overline{\Delta}_\omega = \sup_{t \in \mathbb{R}} f_\omega(t)$. Assume that $\underline{\Delta}_\omega > 0$ for each $\omega \in \Omega$. Moreover assume there exists $\overline{\Delta} > 0$ such that $\sup_{\omega \in \Omega} \overline{\Delta}_\omega \leq \overline{\Delta}$.

Assumptions (A1) and (A2) are necessary for Theorem 2 which provides the uniform conver-

gence of \widehat{F}_ω to F_ω . This is the primary device to overcome the dependence between the summands in the estimator of the transport rank and to establish uniform convergence to the population transport rank. For any $t \in \mathbb{R}$, $F_\omega(t) = \mathbb{E}(\widehat{F}_\omega(t))$. We define functions $y_{\omega,t}(x) = \mathbb{I}\{d(\omega, x) \leq t\} : \Omega \rightarrow \mathbb{R}$ and the function class $\mathcal{F} = \{y_{\omega,t} : \omega \in \Omega, t \in \mathbb{R}\}$. Theorem 2 establishes that under assumptions (A1) and (A2) the function class \mathcal{F} is P -Donsker.

Theorem 2. *Under assumptions (A1) and (A2), $\{\sqrt{n}(\widehat{F}_\omega(t) - F_\omega(t)) : \omega \in \Omega, t \in \mathbb{R}\}$ converges weakly to a zero-mean Gaussian process \mathbb{G}_P with covariance given by*

$$\mathcal{C}_{(\omega_1, t_1), (\omega_2, t_2)} = \text{Cov}(y_{\omega_1, t_1}(X) y_{\omega_2, t_2}(X)).$$

Assumption (A1) is a restriction on the complexity of the metric space (Ω, d) . It is satisfied for a broad class of spaces. Assumption (A2) is a mild regularity condition on the depth profiles.

Any space (Ω, d) such that $\log N(\varepsilon, \Omega, d) = O\left(\frac{1}{\varepsilon^\alpha}\right)$ for some $\alpha < 1$ satisfies Assumption (A1). This is true for any (Ω, d) which can be represented as a subset of elements in a finite dimensional Euclidean space, for example the space of graph Laplacians or network adjacency matrices with fixed number of nodes (Kolaczyk et al. 2020; Ginestet et al. 2017), SPD matrices of a fixed size (Dryden et al. 2009; Thanwerdas and Pennec 2021), simplex valued objects in a fixed dimension (Jeon and Park 2020; Chen et al. 2012) and the space of phylogenetic trees with the same number of tips (Kim et al. 2020; Billera et al. 2001). It holds that $\log N(\varepsilon, \Omega, d) = O(\varepsilon^{-\alpha})$ for any $\alpha < 1$ when Ω is a VC-class of sets or a VC-class of functions (Theorems 2.6.4 and 2.6.7, van der Vaart and Wellner 1996). Assumption (A1) also holds for p -dimensional smooth function classes $C_1^\alpha(\mathcal{X})$ (page 155, van der Vaart and Wellner 1996) on bounded convex sets \mathcal{X} in \mathbb{R}^p equipped with the $\|\cdot\|_\infty$ -norm (Theorem 2.7.1, van der Vaart and Wellner 1996) and $\|\cdot\|_{r,Q}$ -norm for any probability measure Q on \mathbb{R}^p (Corollary 2.7.2, van der Vaart and Wellner 1996), if $\alpha \geq p + 1$.

Of particular interest for many applications is the case when Ω is the space of one-dimensional distributions on some compact interval $I \subset \mathbb{R}$ with the underlying metric $d = d_W$ with d_W being

the 2-Wasserstein metric (Petersen and Müller 2019), defined in (13). If Ω is represented using the quantile function of the distributions then, without any further assumptions, $\log N(\varepsilon, \Omega, d_W)$ is upper and lower bounded by a factor of $1/\varepsilon$ (Proposition 2.1, Blei et al. 2007) and does not meet the criterion in (A1). However, if we assume that the distributions in Ω are absolutely continuous with respect to the Lebesgue measure on I with smooth densities uniformly taking values in some interval $[l_\Omega, u_\Omega]$, then Ω equipped with d_W satisfies (A1). To see this, observe that with the above characterization of Ω the quantile functions corresponding to the distributions in Ω have smooth derivatives that are uniformly bounded. If we let \mathcal{Q}_{deriv} denote the space of the uniformly bounded derivatives of the quantile functions in Ω , then $\log N(\varepsilon, \mathcal{Q}_{deriv}, \|\cdot\|_1) = O(\varepsilon^{-1})$, where $\|\cdot\|_1$ is the L_1 norm under the Lebesgue measure on I (Corollary 2.7.2, van der Vaart and Wellner 1996). Using Lemma 1 in Gao and Wellner (2009), with $\mathcal{F} \equiv \mathcal{Q}_{deriv}$, $\mathcal{G} \equiv \Omega$, $\alpha(x) = x$ and $\phi(\varepsilon) = K/\varepsilon$ for some constant K , $\log N(\varepsilon, \Omega, d_W) = O(\varepsilon^{-1/2})$ which meets the requirement of (A1). If Ω is the space of p -dimensional distributions on a compact convex set $I \subset \mathbb{R}^p$, represented using their distribution functions endowed with the L_r metric with respect to the Lebesgue measure on I , then (A1) is satisfied if $\Omega \subset C_1^\alpha(I)$ for $\alpha \geq p+1$ (see above discussion).

Next we discuss the asymptotic convergence of the estimates \hat{R}_ω of transport rank. Theorem 3 establishes a \sqrt{n} -rate of convergence uniformly in ω for \hat{R}_ω . The proof relies on Corollary 1, which follows from the proof of Theorem 2 and Lemma 1. It follows that the population depth profiles F_ω and the quantile representations F_ω^{-1} and \hat{F}_ω^{-1} are (almost surely) Lipschitz in ω .

Corollary 1. *Under assumptions (A1) and (A2),*

$$\sqrt{n} \sup_{\omega \in \Omega} \sup_{u \in [0,1]} \left| \hat{F}_\omega^{-1}(u) - F_\omega^{-1}(u) \right| = O_{\mathbb{P}}(1).$$

Lemma 1. For any $\omega_1, \omega_2 \in \Omega$ under Assumption (A2),

$$\begin{aligned} \sup_{u \in [0,1]} |F_{\omega_1}^{-1}(u) - F_{\omega_2}^{-1}(u)| &\leq d(\omega_1, \omega_2), \\ \sup_{u \in [0,1]} |\widehat{F}_{\omega_1}^{-1}(u) - \widehat{F}_{\omega_2}^{-1}(u)| &\leq d(\omega_1, \omega_2) \text{ (almost surely) and} \\ \sup_{u \in [0,1]} |F_{\omega_1}(u) - F_{\omega_2}(u)| &\leq \bar{\Delta} d(\omega_1, \omega_2). \end{aligned}$$

Theorem 3. Under assumptions (A1) and (A2),

$$\sqrt{n} \sup_{\omega \in \Omega} |\widehat{R}_\omega - R_\omega| = O_{\mathbb{P}}(1).$$

Next we establish the convergence of the estimated transport median set $\widehat{\mathcal{M}}_\oplus$ to \mathcal{M}_\oplus . Define the Hausdorff metric between $\widehat{\mathcal{M}}_\oplus$ and \mathcal{M}_\oplus as $\rho_H(\widehat{\mathcal{M}}_\oplus, \mathcal{M}_\oplus)$, i.e.,

$$\rho_H(\widehat{\mathcal{M}}_\oplus, \mathcal{M}_\oplus) = \max \left(\sup_{\omega \in \widehat{\mathcal{M}}_\oplus} d(\omega, \mathcal{M}_\oplus), \sup_{\omega \in \mathcal{M}_\oplus} d(\omega, \widehat{\mathcal{M}}_\oplus) \right), \quad (12)$$

where for any $\omega \in \Omega$ and any subset $\mathcal{S} \subset \Omega$, $d(\omega, \mathcal{S}) = \inf_{s \in \mathcal{S}} d(\omega, s)$. We derive

Lemma 2. Under Assumption (A2), for any $\omega_1, \omega_2 \in \Omega$

$$|R_{\omega_1} - R_{\omega_2}| \leq d(\omega_1, \omega_2).$$

Lemma 2 shows uniform Lipschitz continuity of the transport rank R_ω in ω . To proceed, we require an additional assumption.

(A3) For some $\eta' > 0$, for any $0 < \varepsilon < \eta'$, $\alpha(\varepsilon) = \inf_{\tilde{\omega} \in \mathcal{M}_\oplus} \inf_{d(\omega, \tilde{\omega}) > \varepsilon} |R_\omega - R_{\tilde{\omega}}| > 0$.

Theorem 4 below quantifies the asymptotic closeness in the Hausdorff metric of the estimated transport median set and the true transport median set. Assumption (A3) is needed to establish the convergence of the estimated transport median set $\widehat{\mathcal{M}}_\oplus$; it stipulates that the transport ranks

of points outside of ε -neighborhoods of any $\tilde{\omega} \in \mathcal{M}_\oplus$ are well separated from $R_{\tilde{\omega}}$ for a small $\varepsilon > 0$.

Theorem 4. *Assume that the distribution P is such that \mathcal{M}_\oplus is non-empty. Under assumptions (A1)–(A3),*

$$\rho_H(\widehat{\mathcal{M}}_\oplus, \mathcal{M}_\oplus) = o_{\mathbb{P}}(1).$$

5 Simulations

In this and the next section we illustrate the new notions of depth profiles and transport ranks and associated concepts of depth MDS, transport medians and associated quantiles in simulations and data applications for both familiar vector space data and more complex random object data. We start with a simple special case of a Euclidean vector space on more familiar ground.

To this end, we sampled $n = 500$ observations $\{X_i\}_{i=1}^n$ independently from a p -dimensional Gaussian distribution $N(\boldsymbol{\mu}, \boldsymbol{\Sigma})$ for $p = 2$ and $p = 50$, where $\boldsymbol{\mu} = \mathbf{0}$ and $\boldsymbol{\Sigma} = \text{diag}(p, p-1, \dots, 1)$. The depth profiles \widehat{F}_{X_i} (8) and transport ranks \widehat{R}_{X_i} (9) were computed for each observation, adopting the Euclidean metric in \mathbb{R}^p . Irrespective of the type of random objects X_i , the depth profiles \widehat{F}_{X_i} are situated in the space of one-dimensional distributions with finite second moments, which we equip with the Wasserstein metric

$$d_W(F_1, F_2) = \left(\int_0^1 [F_1^{-1}(u) - F_2^{-1}(u)]^2 du \right)^{1/2} = d_{L^2}(F_1^{-1}, F_2^{-1}), \text{ for } F_1, F_2 \in \mathcal{W}. \quad (13)$$

To enhance the graphical illustration of the proposed transport ranks in (4), for implementations, data applications and simulations we partition the observed random objects into $k = 10$ groups according to their transport ranks. Specifically, the range of the transport ranks of observations within a sample $\{X_i\}_{i=1}^n$ is partitioned into k bins, $S_{10} = [0, q_{0.1}]$, $S_9 = (q_{0.1}, q_{0.2}]$, \dots , $S_1 = (q_{0.9}, 1]$, where q_α is the α -quantile of $\{\widehat{R}_{X_i}\}_{i=1}^n$ for $\alpha \in (0, 1)$; then the j -th group consists of observations with transport ranks falling in S_j for $j = 1, \dots, 10$. Arranging the bins in descend-

ing order of transport ranks, these groups are ordered from the innermost to the outermost, providing a center-outward description of the data; we found that the choice $k = 10$ worked well, as illustrated in Figures 3-7 below. The function `CreateDensity()` in the R package `frechet` (Chen et al. 2020) was used to obtain Wasserstein barycenters of depth profiles for each group.

For $p = 2$, the transport ranks (9) based on depth profiles capture the center-outward ordering of the 2-dimensional Gaussian data and the Wasserstein barycenters of the depth profiles within each group shift to the right from group 1 to group 10, where the grouping is as described after eq. (13), reflecting increased distances from the other observations (Figure 3). Figure 4 demonstrates similar findings for a simulated sample of $n = 500$ observations from a 50-dimensional Gaussian distribution $N(\boldsymbol{\mu}, \boldsymbol{\Sigma})$ with $\boldsymbol{\mu} = \mathbf{0}$ and $\boldsymbol{\Sigma} = \text{diag}(50, 49, \dots, 1)$.

Various additional simulation results can be found in the Supplement, including 2-dimensional random vectors generated from multi-modal distributions and comparison with Tukey’s halfspace depth (Tukey 1975) in Section S4; distributional data in Section S5; and a study of robustness of the proposed transport medians (10) in Section S6.

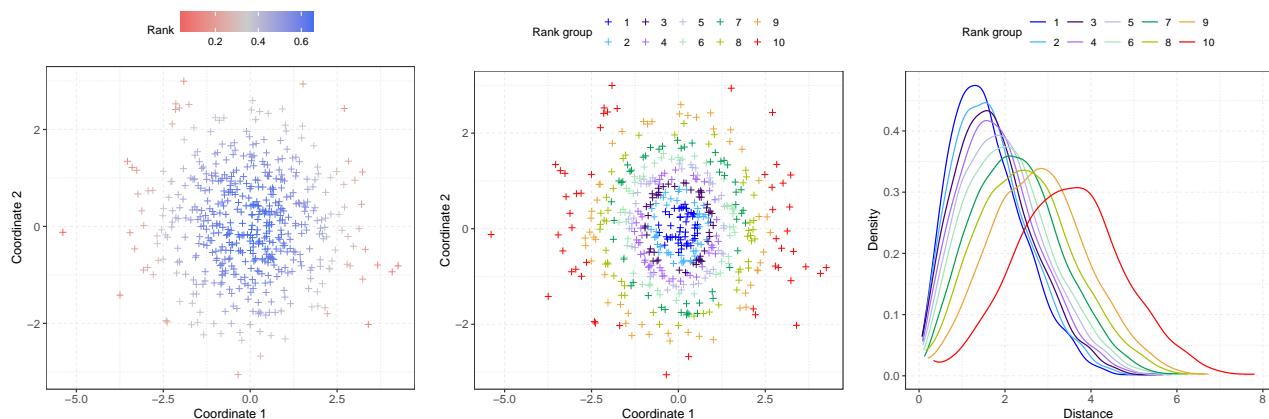


Figure 3: Scatterplots of a sample of $n = 500$ observations generated from a 2-dimensional Gaussian distribution $N(\boldsymbol{\mu}, \boldsymbol{\Sigma})$ with $\boldsymbol{\mu} = \mathbf{0}$ and $\boldsymbol{\Sigma} = \text{diag}(2, 1)$, where the points are colored according to their transport ranks (9) (left) and grouped according to quantiles of transport ranks as described below (13) (middle); Wasserstein barycenters of the depth profiles within each group represented by density functions (right).

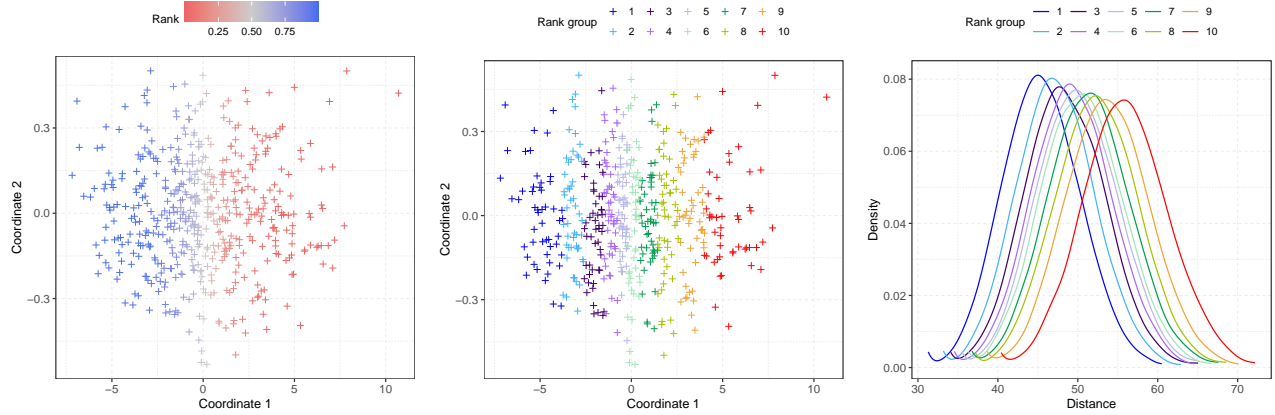


Figure 4: Two-dimensional MDS with respect to the Wasserstein metric d_W in (13) of the depth profiles \hat{F}_{X_i} (8) with $\omega = X_i$ of a sample of $n = 500$ observations generated from a 50-dimensional Gaussian distribution $N(\boldsymbol{\mu}, \boldsymbol{\Sigma})$ with $\boldsymbol{\mu} = \mathbf{0}$ and $\boldsymbol{\Sigma} = \text{diag}(50, 49, \dots, 1)$, where the points are colored according to their transport ranks (9) (left) and grouped according to quantiles of transport ranks as described below (13) (middle); Wasserstein barycenters of the depth profiles within each group represented by density functions (right).

6 Data Applications

6.1 Human Mortality Data

Understanding human longevity has been of long-standing interest and age-at-death distributions are relevant random objects of interest. We consider age-at-death distributions for different countries, which are obtained from the Human Mortality Database (<http://www.mortality.org>) for the year 2000 for $n = 34$ countries/areas, separately for males and females. The age-at-death distributions are shown in the form of density functions in Figure ?? in Section S7 in the supplement. To analyze the data geometry of this sample of distributions $\{X_i\}_{i=1}^{34}$ we adopted the Wasserstein metric and obtained depth profiles \hat{F}_{X_i} (8) with $\omega = X_i$ for each country/area.

For the visualization of these results we introduce *nested circle plots*, shown in the bottom right panels of Figures 5–6. Points representing observations $\{X_i\}_{i=1}^n$ are placed on nested circles such that random objects with transport ranks in the j th bin S_j as determined by the quantiles of transport ranks are located on the j th circle outwards from the center. Therefore, the nested circle

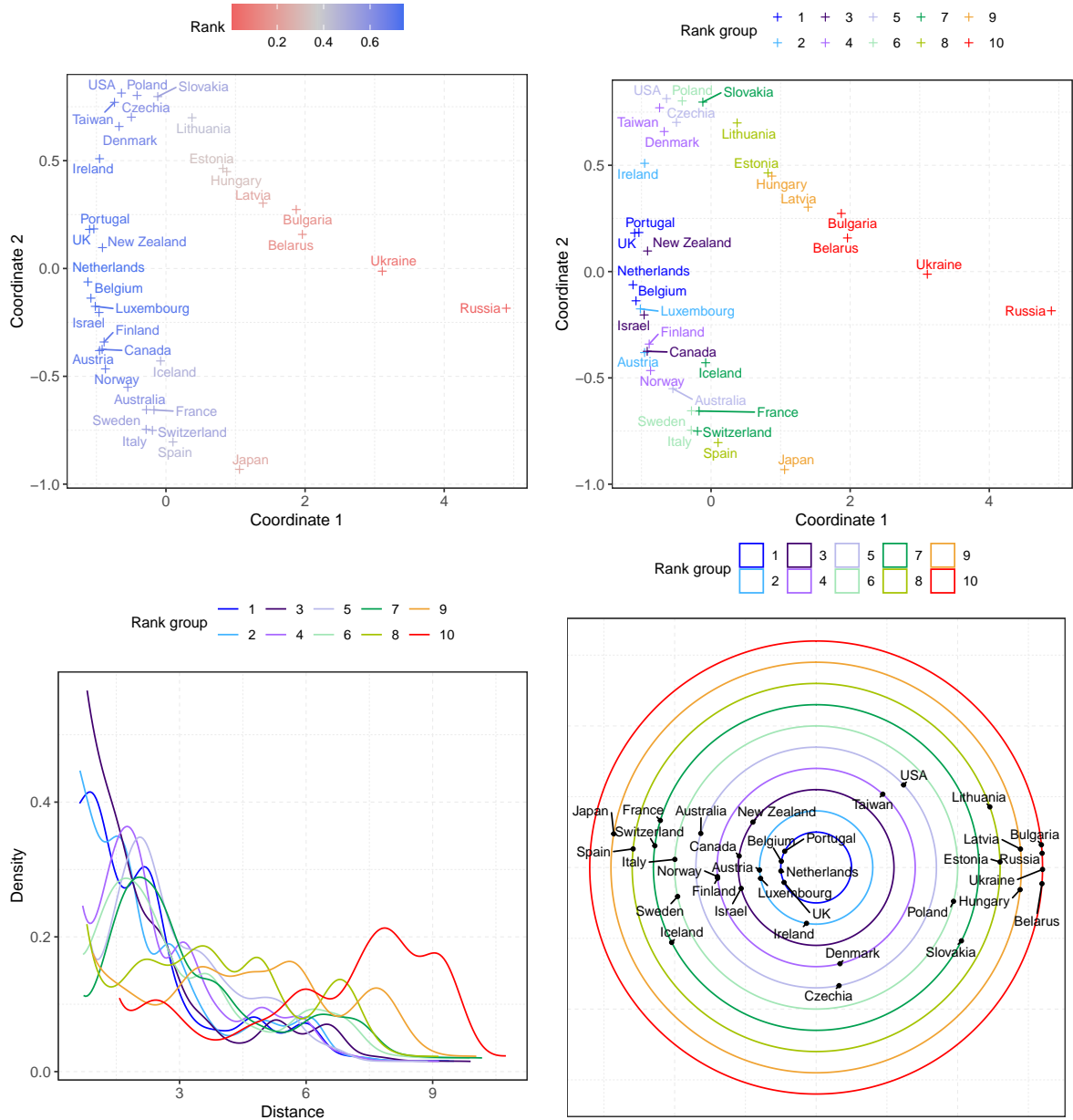


Figure 5: Top: Two-dimensional MDS (Depth MDS) with respect to the Wasserstein metric d_W in (13) of the depth profiles \hat{F}_{X_i} (8) with $\omega = X_i$ of the age-at-death distributions of females in 2000 for the 34 countries, where the points are colored according to their transport ranks (9) (left) and grouped according to quantiles of their transport ranks as described in the text (13) (right). Bottom left: Wasserstein barycenters of the depth profiles \hat{F}_{X_i} for the age-at-death distributions of females in 2000 within each group. Bottom right: Nested circle plot for the age-at-death distributions of females in 2000.

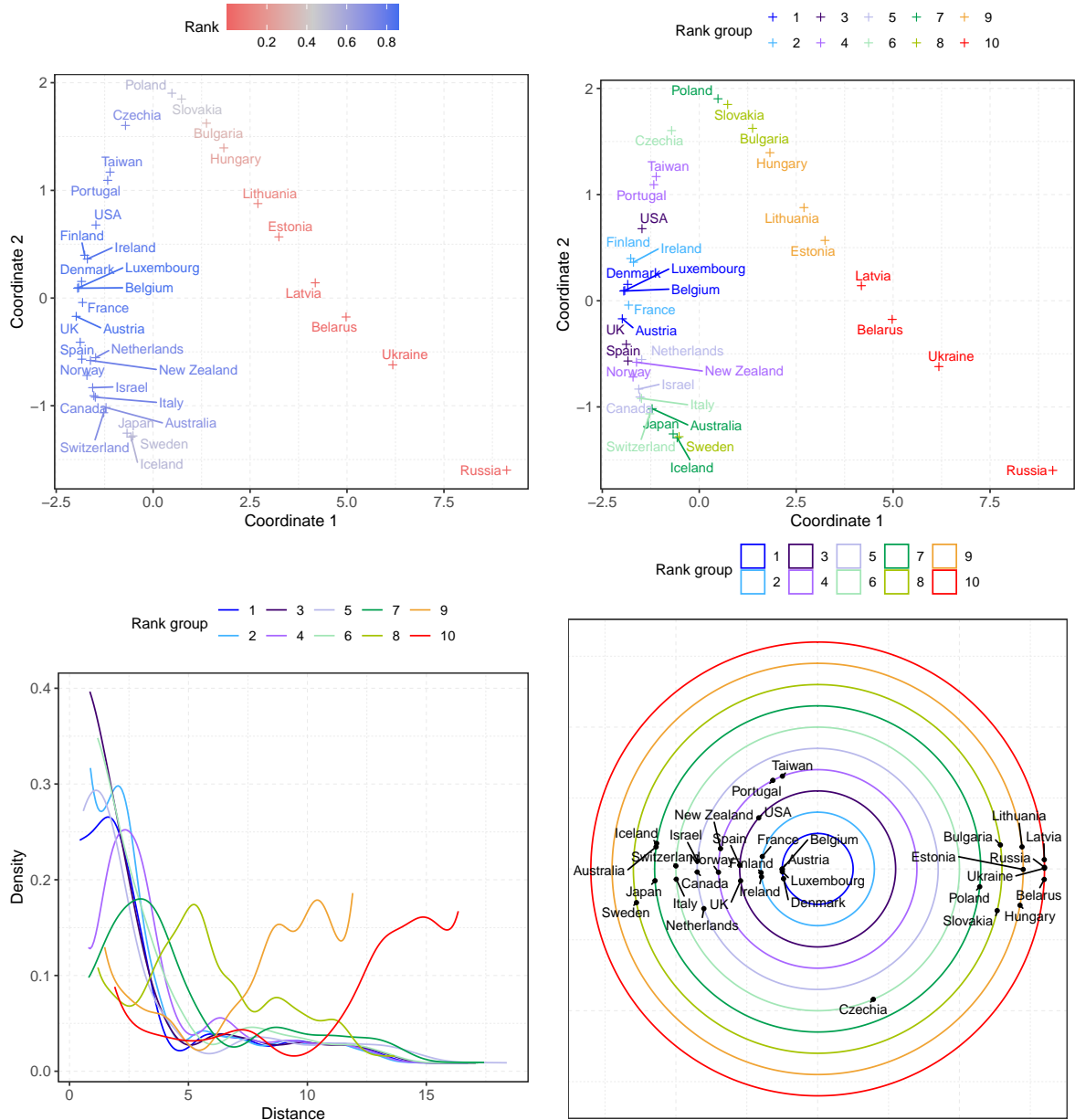


Figure 6: Top: Two-dimensional MDS (Depth MDS) with respect to the Wasserstein metric d_W in (13) of the depth profiles \hat{F}_{X_i} (8) with $\omega = X_i$ of the age-at-death distributions of males in 2000 for the 34 countries, where the points are colored according to their transport ranks (9) (left) and grouped according to quantiles of transport ranks as described in the text (13) (right). Bottom left: Wasserstein barycenters of the depth profiles \hat{F}_{X_i} for the age-at-death distributions of males in 2000 within each group. Bottom right: Nested circle plot for the age-at-death distributions of males in 2000.

positioning reflects the center-outward ordering, with the innermost observations lying on the innermost circle and vice versa. The locations of the observations that fall on the same circle are determined by two-dimensional classical/metric multidimensional scaling (MDS) (Mardia 1978) with respect to the Wasserstein metric d_W (13) of the age-at-death distributions. Specifically, if an observation is mapped to (x, y) by the two-dimensional MDS of the age-at-death distributions, then on the nested circle plot this observation is located at the intersection of the ray $\{(cx, cy) : c > 0\}$ and the corresponding circle, where the MDS step was implemented using the function `cmdscale()` in the R built-in package `stats` (R Core Team 2020). In terms of polar coordinates, angles of points on a nested circle plot are equal to the angles of the corresponding observations on the MDS plot, and radii are determined by the groups to which the observations belong.

These nested circle plots reflect both the similarity of individual observations in terms of their distance in the metric space where the random objects are situated as well as the center-outward ordering as provided by their transport ranks. In the top two panels of Figures 5–6, MDS is applied to the estimated depth profiles \hat{F}_{X_i} with metric d_W , referred to as *depth MDS*, in contrast to *object MDS*, which is applied to the random objects X_i themselves, using the metric d in Ω ; in this particular example both metrics happens to coincide, as $d = d_W$.

For both females and males, two subsets of countries stand out in terms of their depth profiles. One of these subsets includes Japan, while the other subset includes Eastern European countries, such as Russia, Ukraine, Belarus, Latvia and Estonia. While these two subsets are both outlying, the former subset is characterized by enhanced longevity and the latter by reduced longevity. Luxembourg and Belgium belong to the most central group for both females and males. Spain is among the more outlying countries for females only, with advanced longevity increase among females but not males. One can observe many other interesting features for specific countries. Overall, as evidenced in the bottom left panels of Figures 5–6, the age-at-death distributions for males for the outlying countries are more outlying than those for the females. In particular, the empirical Fréchet variance of the depth profiles, $n^{-1} \sum_{i=1}^n d_W^2(\hat{F}_{X_i}, \hat{F}_\oplus)$, of age-

at-death distributions for females and males of different countries is 2.08 and 8.22, respectively, where $\hat{F}_\oplus = \operatorname{argmin}_{\omega \in \mathcal{W}} \sum_{i=1}^n d_W^2(\hat{F}_{X_i}, \omega)$ is the empirical Fréchet mean of the depth profiles.

6.2 U.S. Electricity Generation Data

Compositional data comprise another type of data that do not lie in a vector space. Such data are commonly encountered and consist of vectors of nonnegative elements that sum up to 1. Examples include geochemical compositions and microbiome data. Various approaches to handle the nonlinearity that is inherent in such data have been developed (Aitchison 1986; Sceaaly and Welsh 2014; Filzmoser et al. 2018). We consider here the U.S. electricity generation data which are publicly available on the website of the U.S. Energy Information Administration (<http://www.eia.gov/electricity>). The data consist of net generation of electricity from different sources for each state. Here, we consider the data for the year 2000. In preprocessing, we excluded the “pumped storage” category due to errors in these data and then merged the energy sources into three categories: Natural Gas, consisting of “natural gas” alone; Other Fossil, consisting of “coal”, “petroleum” and “other gases”; Renewables and Nuclear, combining the remaining sources “hydroelectric conventional”, “solar thermal and photovoltaic”, “geothermal”, “wind”, “wood and wood derived fuels”, “other biomass”, “nuclear” and “other”. Hence, we have a sample of $n = 50$ observations $\{X_i\}_{i=1}^n$, each of which takes values in a 2-simplex $\Delta^2 = \{\mathbf{x} \in \mathbb{R}^3 : \mathbf{x}^\top \mathbf{1}_3 = 1\}$, where $\mathbf{1}_3 = (1, 1, 1)^\top$. Since the component-wise square root $\sqrt{\mathbf{x}} = (\sqrt{x_1}, \sqrt{x_2}, \sqrt{x_3})^\top$ of an element $\mathbf{x} \in \Delta^2$ lies in the sphere \mathcal{S}^2 , we adopt the geodesic metric on this sphere

$$d_S(\mathbf{x}, \mathbf{y}) = \arccos(\sqrt{\mathbf{x}}^\top \sqrt{\mathbf{y}}), \text{ for } \mathbf{x}, \mathbf{y} \in \Delta^2. \quad (14)$$

We then compared the estimated transport ranks (9) for each state with the angular Tukey depths (ATDs, Liu and Singh 1992) of $\{\sqrt{X_i}\}_{i=1}^n$. At a first glance, the proposed transport ranks and ATDs yield similar center-outward ordering of the 50 states for these data (Figure 7).

Maryland emerges as the transport median and is also at the median in terms of ATDs. On closer inspection, one finds some interesting discrepancies between transport ranks and the ATDs, especially for the states that are either close to or far away from the center Maryland in terms of their outlyingness. The states near Maryland, as shown in orange and light violet in the bottom panels of Figure 7, all have high transport ranks, while their ATDs vary widely. In particular, Montana, with an electricity generation pattern very similar to that of Maryland, has the lowest ATD level while it has a high transport rank. A subset of states that are colored in turquoise and light violet in the bottom panels of Figure 7 have the lowest ATDs among all states but have a much wider range of transport ranks. For example, Hawaii and Delaware for which energy sources are similar to those of Maryland have high transport ranks and low ATD levels. The overall conclusion is that transport ranks are better suited than ATDs for studying the geometry of this data set and for quantifying outlyingness.

Networks as random objects are illustrated in a third data application for New York taxi trips, with details in Section S8 of the Supplement.

7 Discussion

In this paper we introduce a new toolbox for the analysis of metric space valued data referred to as random objects. Key elements of this toolbox are depth profiles, transport ranks and transport median sets. Depth profiles are canonical and surprisingly simple. In combination with optimal transport they lead to the notion of transport ranks, which can then be harnessed to arrive at a novel notion of data depth that is even of interest for the classical case of multivariate Euclidean data. Depth profiles can be viewed as a representation of random objects in the context of their underlying probability distribution and under mild conditions characterize this distribution.

We explore here only some of the most salient of the numerous concepts that they engender, which include depth MDS; transport modes; depth level sets that can be harnessed to obtain tolerance regions for a specified level; and depth quantiles. Especially the latter is an important

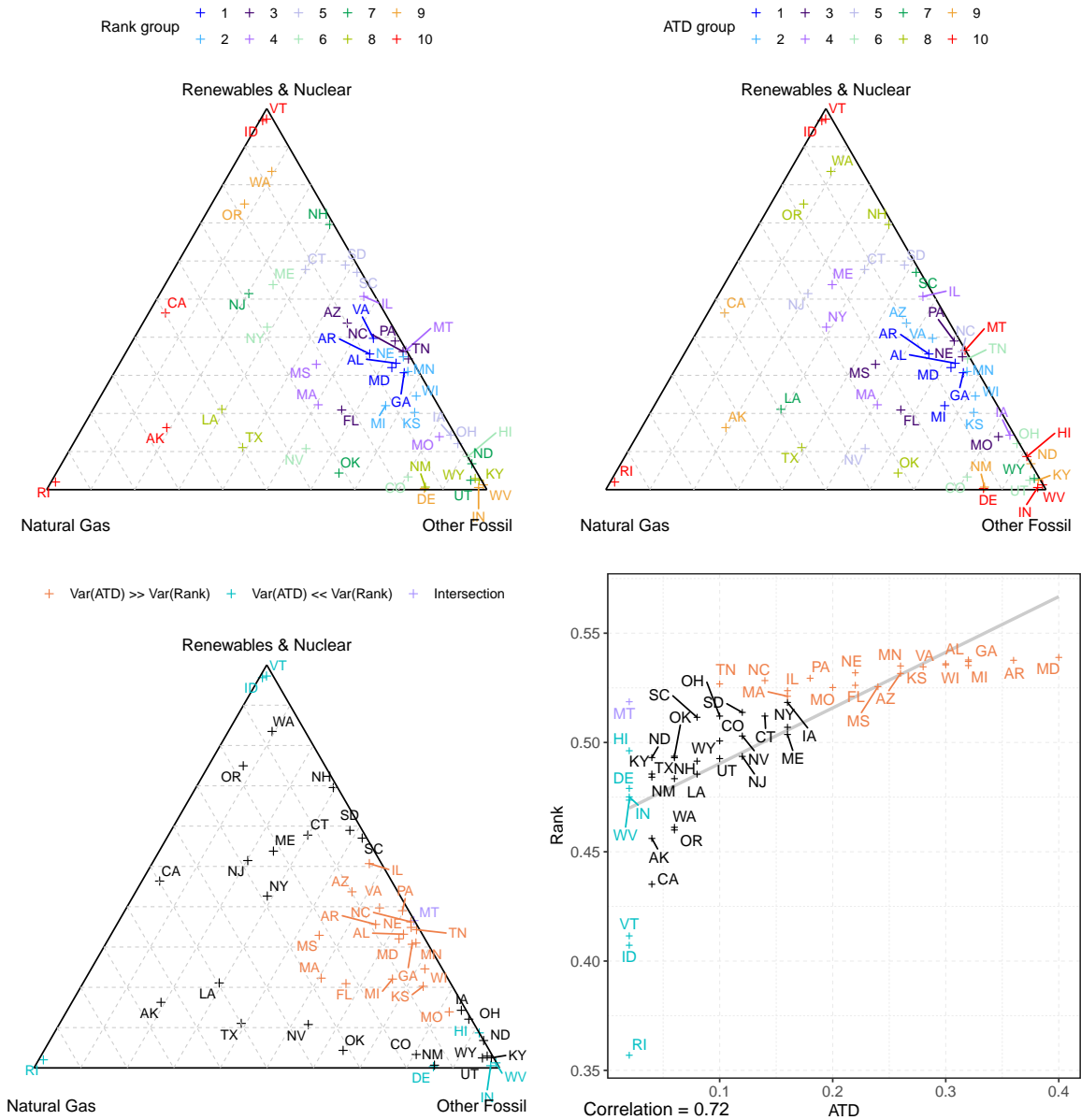


Figure 7: Ternary plot of compositions of electricity generation in the year 2000 for the 50 states in the U.S., where the points are colored as per their grouping according to quantiles of transport ranks as described in the text (13) (top left); the corresponding grouping based on angular Tukey depths (ATDs, top right); highlighted subsets that show differences between transport ranks and ATDs (bottom left); and a scatterplot of transport ranks (9) versus ATDs (bottom right), where the straight line shows the least squares fit (to provide perspective) and the Pearson correlation between the transport ranks and ATDs is 0.727. In the bottom two panels, a subset of states with similarly small ATDs but varying transport ranks is highlighted in orange, and another subset with similarly high transport ranks but varying ATDs is highlighted in turquoise, where the intersection of these two subsets is colored in light violet.

as well as elusive and hard to conceptualize notion for random objects. We note that in contrast to the more standard object MDS the new depth MDS depicted in Figure for the human mortality data reveals interesting dimension reduction aspects through the horseshoe shape of two-dimensional depth MDS plot; see also [Chen and Müller \(2012\)](#) for further discussion of such horseshoes in the context of manifold learning and also Figure ?? in the Supplement.

Apart from opening a new arena for future explorations of general metric space valued data, the proposed toolbox is also of interest for revisiting data analysis in classical Euclidean spaces, as transport depth that has not yet been explored in these more traditional spaces, which also include infinite-dimensional Hilbert spaces that are commonly used for modeling functional data. We also introduce sample-based estimators for the population based concepts, which can be easily and efficiently constructed. Theoretical analysis shows that these estimators converge to their population targets. Additional simulations in the Supplement provide evidence that the proposed transport ranks can give rise to more adequate perspectives compared to the well-established Tukey’s half depth rank in the special case where the data are situated in a Euclidean vector space and furthermore that transport medians outperform Fréchet means in terms of robustness.

The supporting theory applies to a wide class of metric space and probability measure combinations, as long as an entropy condition is satisfied and the metric space is totally bounded (and separable, which is implied by total boundedness). While this does place a restriction on the space/measure combinations for which the theory applies, we show that most object spaces of practical interest such as distributional data, networks and tree spaces are covered under mild regularity conditions. From a practical perspective, as long as one can compute pairwise distances, the proposed tools can be applied for the exploratory and geometric analysis of metric space valued data; a pertinent example is the detection of outliers.

Various extensions will be of interest for future research. For example, to understand the interplay between depth profiles and distances between objects in Ω one may work with gener-

alizations of the transport rank R_ω , the *generalized transport rank* R_ω^ψ , as

$$R_\omega^\psi = \text{expit} \left[\mathbb{E} \left\{ \psi(d(\omega, X)) \int_0^1 [F_X^{-1}(u) - F_\omega^{-1}(u)] \, du \right\} \right]$$

where $\psi(\cdot)$ is a weight function which can be tuned depending on the goal of the data analysis. Through the choice of ψ one may emphasize either observations closer or farther from ω . One could also consider alternative definitions of transport ranks based on depth profiles, e.g., by adopting various distributional metrics $m(F_X, F_\omega)$ to gauge the distance between depth profiles.

References

- Aitchison, J. (1986). *The Statistical Analysis of Compositional Data*. Chapman & Hall, Ltd.
- Ambrosio, L., N. Gigli, and G. Savaré (2008). *Gradient Flows in Metric Spaces and in the Space of Probability Measures*. Springer.
- Barnett, V. (1976). The ordering of multivariate data. *Journal of the Royal Statistical Society: Series A (General)* 139(3), 318–344.
- Billera, L. J., S. P. Holmes, and K. Vogtmann (2001). Geometry of the space of phylogenetic trees. *Advances in Applied Mathematics* 27(4), 733–767.
- Blei, R., F. Gao, and W. Li (2007). Metric entropy of high dimensional distributions. *Proceedings of the American Mathematical Society* 135(12), 4009–4018.
- Cascos, I., Q. Li, and I. Molchanov (2021). Depth and outliers for samples of sets and random sets distributions. *Australian & New Zealand Journal of Statistics* 63(1), 55–82.
- Chau, J., H. Ombao, and R. von Sachs (2019). Intrinsic data depth for Hermitian positive definite matrices. *Journal of Computational and Graphical Statistics* 28(2), 427–439.
- Chavel, I. (2006). *Riemannian Geometry: A Modern Introduction*. Cambridge: Cambridge University Press.
- Chen, D. and H.-G. Müller (2012). Nonlinear manifold representations for functional data. *The Annals of Statistics* 40, 1–29.
- Chen, J., K. Bittinger, E. S. Charlson, C. Hoffmann, J. Lewis, G. D. Wu, R. G. Collman, F. D. Bushman, and H. Li (2012). Associating microbiome composition with environmental covariates using generalized UniFrac distances. *Bioinformatics* 28(16), 2106–2113.
- Chen, M., C. Gao, and Z. Ren (2018). Robust covariance and scatter matrix estimation under Huber’s contamination model. *The Annals of Statistics* 46(5), 1932–1960.

- Chen, Y., A. Gajardo, J. Fan, Q. Zhong, P. Dubey, K. Han, S. Bhattacharjee, and H.-G. Müller (2020). *frechet: Statistical Analysis for Random Objects and Non-Euclidean Data*. R package version 0.2.0, available at <https://CRAN.R-project.org/package=frechet>.
- Cholaquidis, A., R. Fraiman, F. Gamboa, and L. Moreno (2020). Weighted lens depth: Some applications to supervised classification. *arXiv preprint arXiv:2011.11140*.
- Claeskens, G., M. Hubert, L. Slaets, and K. Vakili (2014). Multivariate functional halfspace depth. *Journal of the American Statistical Association* 109(505), 411–423.
- Dai, X. and S. Lopez-Pintado (2021). Tukey’s depth for object data. *Journal of the American Statistical Association arXiv preprint arXiv:2109.00493*.
- De Micheaux, P. L., P. Mozharovskiy, and M. Vimond (2021). Depth for curve data and applications. *Journal of the American Statistical Association* 116(536), 1881–1897.
- Dryden, I. L., A. Koloydenko, and D. Zhou (2009). Non-Euclidean statistics for covariance matrices, with applications to diffusion tensor imaging. *The Annals of Applied Statistics* 3, 1102–1123.
- Dutta, S., A. K. Ghosh, and P. Chaudhuri (2011). Some intriguing properties of Tukey’s half-space depth. *Bernoulli* 17(4), 1420–1434.
- Dyckerhoff, R. (2004). Data depths satisfying the projection property. *Allgemeines Statistisches Archiv* 88(2), 163–190.
- Filzmoser, P., K. Hron, and M. Templ (2018). *Applied Compositional Data Analysis: With Worked Examples in R*. Springer.
- Fraiman, R. and G. Muniz (2001). Trimmed means for functional data. *Test* 10(2), 419–440.
- Fréchet, M. (1948). Les éléments aléatoires de nature quelconque dans un espace distancié. *Annales de l’Institut Henri Poincaré* 10, 215–310.
- Gao, F. and J. A. Wellner (2009). On the rate of convergence of the maximum likelihood estimator of a k-monotone density. *Science in China Series A: Mathematics* 52(7), 1525–1538.
- Geenens, G., A. Nieto-Reyes, and G. Francisci (2021). Statistical depth in abstract metric spaces. *arXiv preprint arXiv:2107.13779*.
- Ghosh, A. K. and P. Chaudhuri (2005). On maximum depth and related classifiers. *Scandinavian Journal of Statistics* 32(2), 327–350.
- Gijbels, I. and S. Nagy (2017). On a general definition of depth for functional data. *Statistical Science* 32(4), 630–639.
- Ginestet, C. E., J. Li, P. Balachandran, S. Rosenberg, and E. D. Kolaczyk (2017). Hypothesis testing for network data in functional neuroimaging. *The Annals of Applied Statistics*, 725–750.
- Jeon, J. M. and B. U. Park (2020). Additive regression with Hilbertian responses. *The Annals of Statistics* 48(5), 2671–2697.

- Jörnsten, R. (2004). Clustering and classification based on the L_1 data depth. *Journal of Multivariate Analysis* 90(1), 67–89.
- Kim, J., N. A. Rosenberg, and J. A. Palacios (2020). Distance metrics for ranked evolutionary trees. *Proceedings of the National Academy of Sciences* 117(46), 28876–28886.
- Kleindessner, M. and U. von Luxburg (2017). Lens depth function and k -relative neighborhood graph: Versatile tools for ordinal data analysis. *Journal of Machine Learning Research* 18(58), 1–52.
- Kolaczyk, E. D., L. Lin, S. Rosenberg, J. Walters, and J. Xu (2020). Averages of unlabeled networks: Geometric characterization and asymptotic behavior. *The Annals of Statistics* 48(1), 514–538.
- Koshevoy, G. and K. Mosler (1997). Zonoid trimming for multivariate distributions. *The Annals of Statistics* 25(5), 1998–2017.
- Lange, T., K. Mosler, and P. Mozharovskiy (2014). Fast nonparametric classification based on data depth. *Statistical Papers* 55(1), 49–69.
- Li, J., J. A. Cuesta-Albertos, and R. Y. Liu (2012). DD-classifier: Nonparametric classification procedure based on DD-plot. *Journal of the American Statistical Association* 107(498), 737–753.
- Li, J. and R. Y. Liu (2004). New nonparametric tests of multivariate locations and scales using data depth. *Statistical Science* 19(4), 686–696.
- Lin, Z. and H.-G. Müller (2021). Total variation regularized Fréchet regression for metric-space valued data. *The Annals of Statistics* 49, 3510–3533.
- Liu, R. Y. (1990). On a notion of data depth based on random simplices. *The Annals of Statistics* 18(1), 405–414.
- Liu, R. Y., J. M. Parelius, and K. Singh (1999). Multivariate analysis by data depth: Descriptive statistics, graphics and inference (with discussion and a rejoinder by Liu and Singh). *The Annals of Statistics* 27(3), 783–858.
- Liu, R. Y. and K. Singh (1992). Ordering directional data: Concepts of data depth on circles and spheres. *The Annals of Statistics* 20(3), 1468–1484.
- Liu, Z. and R. Modarres (2011). Lens data depth and median. *Journal of Nonparametric Statistics* 23(4), 1063–1074.
- Liu, Z., R. Modarres, and M. Yang (2013). A multivariate control quantile test using data depth. *Computational Statistics & Data Analysis* 57(1), 262–270.
- López-Pintado, S. and J. Romo (2009). On the concept of depth for functional data. *Journal of the American Statistical Association* 104(486), 718–734.
- López-Pintado, S. and J. Romo (2011). A half-region depth for functional data. *Computational*

- Statistics & Data Analysis* 55(4), 1679–1695.
- Lunagómez, S., S. C. Olhede, and P. J. Wolfe (2020). Modeling network populations via graph distances. *Journal of the American Statistical Association*, 1–18.
- Lyons, R. (2013). Distance covariance in metric spaces. *Annals of Probability* 41(5), 3284–3305.
- Mardia, K. V. (1978). Some properties of classical multi-dimensional scaling. *Communications in Statistics - Theory and Methods* 7(13), 1233–1241.
- Mosler, K. (2013). Depth statistics. In C. Becker, R. Fried, and S. Kuhnt (Eds.), *Robustness and Complex Data Structures*, pp. 17–34. Springer.
- Mosler, K. and P. Mozharovskyi (2021). Choosing among notions of multivariate depth statistics. *Statistical Science*. in press.
- Mosler, K. and Y. Polyakova (2012). General notions of depth for functional data. *arXiv preprint arXiv:1208.1981*.
- Nagy, S., I. Gijbels, M. Omelka, and D. Hlubinka (2016). Integrated depth for functional data: Statistical properties and consistency. *ESAIM: Probability and Statistics* 20, 95–130.
- Nieto-Reyes, A. and H. Battey (2016). A topologically valid definition of depth for functional data. *Statistical Science* 31(1), 61–79.
- Oja, H. (1983). Descriptive statistics for multivariate distributions. *Statistics & Probability Letters* 1(6), 327–332.
- Paindaveine, D. and G. Van Bever (2013). From depth to local depth: A focus on centrality. *Journal of the American Statistical Association* 108(503), 1105–1119.
- Paindaveine, D. and G. Van Bever (2018). Halfspace depths for scatter, concentration and shape matrices. *The Annals of Statistics* 46(6B), 3276–3307.
- Petersen, A. and H.-G. Müller (2019). Fréchet regression for random objects with euclidean predictors. *The Annals of Statistics* 47(2), 691–719.
- R Core Team (2020). *R: A Language and Environment for Statistical Computing*. Vienna, Austria: R Foundation for Statistical Computing.
- Rousseeuw, P. J. and M. Hubert (1999). Regression depth. *Journal of the American Statistical Association* 94(446), 388–402.
- Rousseeuw, P. J., I. Ruts, and J. W. Tukey (1999). The bagplot: A bivariate boxplot. *The American Statistician* 53(4), 382–387.
- Scealy, J. and A. Welsh (2014). Colours and cocktails: Compositional data analysis. *Australian & New Zealand Journal of Statistics* 56(2), 145–169.
- Serfling, R. (2002). A depth function and a scale curve based on spatial quantiles. In *Statistical Data Analysis Based on the L_1 -Norm and Related Methods*, pp. 25–38. Springer.
- Thanwerdas, Y. and X. Pennec (2021). $O(n)$ -invariant Riemannian metrics on SPD matrices.

arXiv preprint arXiv:2109.05768.

- Tukey, J. W. (1975). Mathematics and the picturing of data. In *Proceedings of the International Congress of Mathematicians*, Volume 2, pp. 523–531. Canadian Mathematical Congress.
- van der Vaart, A. and J. Wellner (1996). *Weak Convergence and Empirical Processes*. Springer, New York.
- Wang, X., J. Zhu, W. Pan, J. Zhu, and H. Zhang (2021). Nonparametric statistical inference via metric distribution function in metric spaces. *arXiv preprint arXiv:2107.07317*.
- Yang, M. and R. Modarres (2018). β -skeleton depth functions and medians. *Communications in Statistics—Theory and Methods* 47(20), 5127–5143.
- Zhang, J. (2002). Some extensions of Tukey’s depth function. *Journal of Multivariate Analysis* 82(1), 134–165.
- Zuo, Y. and R. Serfling (2000). General notions of statistical depth function. *The Annals of Statistics* 28(2), 461–482.